Microchimica Acta (2020) 187: 468
https://doi.org/10.1007/s00604-020-04431-3

ORIGINAL PAPER

Hollow sphere nickel sulfide nanostructures–based enzyme mimic electrochemical sensor platform for lactic acid in human urine

Mani Arivazhagan[1] · Ayyavu Shankar[1] · Govindhan Maduraiveeran[1]

Received: 25 February 2020 / Accepted: 7 July 2020 / Published online: 22 July 2020
© Springer-Verlag GmbH Austria, part of Springer Nature 2020

Abstract

An enzyme-free electrochemical sensor platform is reported based on hollow sphere structured nickel sulfide (HS-NiS) nanomaterials for the sensitive lactic acid (LA) detection in human urine. Hollow sphere nickel sulfide nanostructures directly grow on the nickel foam (NiF) substrate by using facile and one-step electrochemical deposition strategy towards the electrocatalytic lactic acid oxidation and sensing for the first time. The as-developed nickel sulfide nanostructured electrode (NiF/HS-NiS) has been successfully employed as the enzyme mimic electrode towards the enhanced electrocatalytic oxidation and detection of lactic acid. The NiF/HS-NiS electrode exhibits an excellent electrocatalytic activity and sensing ability with low positive potential (~ 0.52 V vs Ag/AgCl), catalytic current density (~ 1.34 mA), limit of detection (LOD) (0.023 μM), linear range from 0.5 to 88.5 μM with a correlation coefficient of $R^2 = 0.98$, sensitivity (0.655 μA μM^{-1} cm^{-2}), and selectivity towards the lactic acid owing to the ascription of high inherent electrical conductivity, large electrochemical active surface area (ECASA), high electrochemical active sites, and strong adsorption ability. The sensors developed in this work demonstrate the selectivity against potential interferences, including uric acid (UA), ascorbic acid (AA), paracetamol (PA), Mg^{2+}, Na^{+}, and Ca^{2+}. Furthermore, the developed sensors show practicability by sensing lactic acid in human urine samples, suggesting that the HS-NiS nanostructures device has promising clinical diagnostic potential.

Keywords Nickel sulfide · Hollow architecture · Nanostructures · Modified electrode · Electrocatalysis · Lactic acid detection

Introduction

The detection of chemically and biologically active species is vital in the area of healthcare and medical diagnosis [1–3]. Numerous enzymatic biosensors were developed for the detection and determination of biomarkers, including glucose, NADH, H_2O_2, cholesterol, lactic acid (LA), etc. through either in vitro or in vivo investigations [4–9]. In particular, lactic acid biosensors are in highly in-demand in various applications such as clinical analysis, biomedical, biological, food industries, and sports for the rapid detection and determination of lactic acid levels in our bodily fluids [10–14]. The elevated concentrations of lactic acid may not only specify the existence but also indicate the harshness of clinically imperative disorders [12]. Consequently, it is required to design a lactic acid sensor gifted with simplicity to prepare, quickness in response time, low cost, high selectivity, and high sensitivity. Due to the several demerits of the enzyme-based biosensor [15–20], a new design of electrochemical sensors with artificial or enzyme mimic catalysts received much attention. Alongside enzyme-based electrochemical biosensors, the enzyme-free sensors are getting excessive consideration due to the advantages of cost-effective fabrication, enhanced electrochemical redox properties, durability and good reproducibility, etc. [21, 22].

Recently, numerous enzyme-free electrochemical sensors based on various nanostructured materials such as noble metal nanoparticles of gold (Au), platinum (Pt), and silver (Ag) and its alloy–metals [23–25] and transition metal oxides such as nickel oxide (NiO), copper oxide (CuO), manganese oxide (MnO_2), and Co_3O_4 were developed [26]. Recently, transition metal chalcogenides (TMC) were considered as promising

Electronic supplementary material The online version of this article (https://doi.org/10.1007/s00604-020-04431-3) contains supplementary material, which is available to authorized users.

✉ Govindhan Maduraiveeran
maduraig@srmist.edu.in

[1] Materials Electrochemistry Laboratory, Department of Chemistry, SRM Institute of Science and Technology, Kattankulathur, Tamil Nadu 603 203, India

candidates due to their low cost, ease of biocompatible, and layer- and morphological-dependent physico-chemical characteristics [27, 28]. Transition metal chalcogenides have been employed in many potential applications, including electrochemical sensors, electrocatalysis, high-performance supercapacitors, and lithium-ion batteries [29, 30]. In particular, binary nickel sulfides (NiS) possessed enhanced electrocatalytic properties through high electronic conductivity, rich redox chemistry, different atomic configurations, and crystalline structures [31, 32]. For instance, Liu Co-workers developed the various crystal phases and morphologies of NiS_x through the solvothermal reaction, exhibiting various structure dependent-electrocatalytic properties [33]. Zhang Co-workers reported the microwave-assisted synthesis of NiS_2 with controlled morphologies such as nanocubes, nanospheres, and nanoparticles [34]. Therefore, the development of high-performance and enzyme mimic electrochemical lactic acid sensor based on NiS nanostructures is a key.

In the present study, a novel hollow sphere-architectured NiS nanomaterial was directly grown on NiF substrate for the sensitive lactic acid detection in human urine for the first time. To our knowledge, the present enzyme-free electrochemical sensor possessed several advantages, including (i) one-step and simple electrochemical fabrication of sensing electrode strategy; (ii) growing hollow sphere-architectured NiS nanomaterials with high dense NiS clusters (~ 2.0 nm) with free of any templates/capping agents; (iii) time-effective and a green strategy without using of any organic solutions; and (iv) enzyme mimic electrocatalytic activity towards the sensitive detection of lactic acid.

Experimental section

Reagents and solutions

Nickel(II)nitrate hexahydrate ($Ni(NO_3)_2.6H_2O$) was purchased from the Sisco laboratory. Potassium hydroxide pellets (KOH) were purchased from Emplura. Thiourea was purchased from Alfa Aeser. Nitric acid (HNO_3) was purchased from Rankem analytic. Lactic acid, uric acid, ascorbic acid, paracetamol, magnesium sulfate hexahydrate, sodium chloride, and calcium sulfate pentahydrate were obtained from Sigma Aldrich. All reagents purchased and utilized in this study were of analytical grade and utilized without further purification. Millipore Milli-Q nanopure water (resistivity ≥ 18 MΩ cm) was employed for the preparation of all solutions.

Characterization of hollow sphere NiS nanostructures

The crystal structures of the as-prepared hollow sphere NiS nanomaterials were primarily characterized using X-ray diffraction (XRD) technique with a Pananalytical Xpert Pro Diffractometer. The surface morphology of the hollow sphere NiS nanomaterials was characterized using a high-resolution scanning electron microscope (FE-SEM) with an FEI Quanta FEG 200, and a high-resolution transmission electron microscope (HR-TEM) with a JEOL 2010F TEM. The elemental composition and distribution of the hollow sphere NiS nanomaterials were studied by using electron dispersive X-ray (EDX) techniques with Hitachi SU-70. X-ray photoelectron spectroscopic measurements were performed to understand the chemical compositions and the valence states of hollow sphere NiS nanomaterials using a XPS-PHI Versaprobe III.

Electrochemical measurements

All the electrochemical measurements were conducted by employing an Electrochemical Bio Logic SP-300 workstation out at an ambient temperature of 25 ± 3 °C. The NiF modified with HS-NiS nanomaterials was used as the working electrode, a platinum wire employed as the counter electrode and Ag/AgCl (3.0 M KCl) electrode used as the reference electrode. Cyclic voltammetric (CV) technique was employed to study the electrochemical properties and electrocatalytic properties of the NiF/HS-NiS electrode. Chronoamperometric (CA) technique was utilized for the sensing performance of the NiF/HS-NiS electrode.

Electrochemical sensor fabrication

Electrochemical deposition strategy was adopted to fabricate HS-NiS nanostructures. The pre-cleaned NiF substrate (surface area of ~ 0.18 cm^2) was employed as the working electrode to deposit the HS-NiS. Initially, the NiF was cleaned by 3 min sonication in acetone and pure water before to electrochemical deposition process. Typically, there are five continuous electrochemical cyclings of the potential window, starting from 0.6 to − 1.2 V (vs Ag/AgCl) in the mixture of 5.0 mM Ni salt precursor + 0.75 M thiourea + 0.1 M nitric acid at a scan rate of 5.0 mV s^{-1} (Fig. S1). The electrochemical deposited hollow-structured NiS nanomaterials on NiF, designated as NiF/HS-NiS. The mass loading of HS-NiS was estimated to be 0.024 mg. The developed NiF/HS-NiS electrode will be employed as the sensing electrode for the detection of lactic acid under alkaline electrolytes.

Preparation of actual human urinary sample

An original human urine sample was collected from a healthy volunteer (~ 24 years old) and stored in the refrigerator immediately. A small volume (~ 5.0 mL) serum sample was then centrifuged for 30 min. The supernatant was filtered and then diluted ~ 10 times using 1.0 M KOH. The resulting solution was transferred into the electrochemical cell for real sample analysis without any further pretreatment. A stock solution of lactic acid (1.0 mM) was stored in a refrigerator, which was further diluted

to obtain 0.5, 1.0, and 2.0 μM of lactic acid. For the lactic acid determination in urine samples, the standard addition method (SAM) was employed for the detection of lactic acid concentrations ranged from 0.5 to 2.0 μM. Chronoamperometric technique was used to perform the recovery test for the detection and determination of lactic acid in the human urine samples by adding a defined concentration of lactic acid. Based on our controlled amperometric studies, the concentration of lactic acid is negligible or zero concentration in the actual urine samples.

Results and discussion

Morphological characterization of hollow sphere NiS nanostructures

Figure 1 presents the typical FE-SEM images of the developed hollow sphere-structured NiS nanomaterials with low (A) and high (B) magnifications. The average size of the formed hollow sphere NiS nanomaterials was calculated to be ~ 184.0 nm with hollow size of ~ 93.0 nm as shown in Fig. 1. As can be easily seen in Fig. 1(A), the hollow sphere NiS nanomaterials were homogeneously distributed using a single step electrochemical deposition method. As depicted in Fig. S1, the CVs of the NiF electrode recorded in the electrolyte solution of 5.0 mM Ni precursor + 0.75 M thiourea + 0.1 M nitric acid at a scan rate of 5.0 mV s^{-1} for five continuous cycles. During the electrochemical deposition, the formed $Ni(CH_4N_2S)_2^{2+}$ was then reduced to form HS-NiS on the NiF substrate as given in Eqs. (1) and (2) [33]. It may be anticipated the so-formed $Ni(CH_4N_2S)_2^{2+}$ primarily on edge of the pores of NiF, and grown as hollow sphere NiS nanostructures on the NiF substrate.

$$Ni^{2+} + 2(CH_3N_2S) \rightarrow Ni(CH_3N_2S)_2^{2+} \quad (1)$$

$$Ni(CH_3N_2S)_2^{2+} + H_2O + 2e^- \rightarrow NiS \quad (2)$$

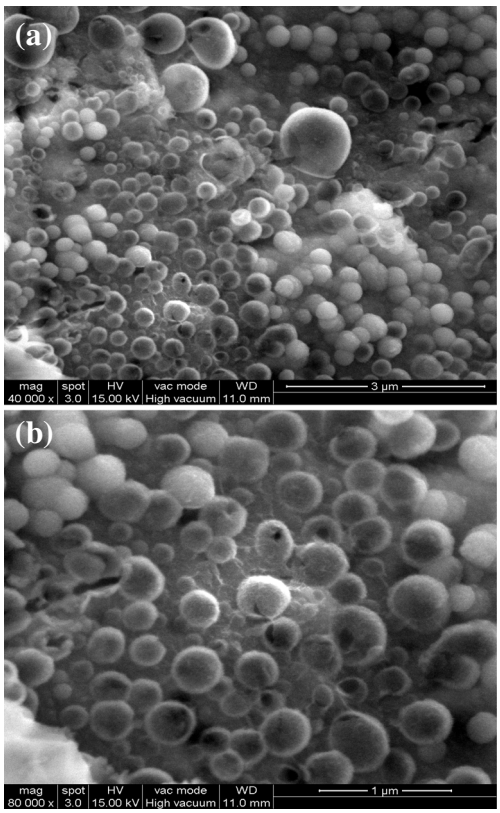

Fig. 1 FE-SEM images of the NiF/HS-NiS electrode with low (**a**) and high (**b**) magnifications

The atomic ratio of Ni to S was measured to be 68.2:31.8 for the hollow sphere NiS nanomaterials using the EDX spectrum of the hollow sphere NiS nanomaterials (Fig. S2). The elementals of Ni and S were homogenously distributed in hollow sphere NiS nanomaterials as depicted in Fig. S3. Figure 2 displays the TEM, HR-TEM, and selected area electron diffraction (SAED) pattern of the developed hollow sphere NiS nanomaterials. As depicted in Figs. 2(A) and S4, the sphere-like NiS has the dimension of ~ 130.0 nm, and the size of hollow was found to be ~ 35.0 nm, which agrees with the FE-SEM results of Fig. 1. The hollow structure of the NiS was found based on the bright-field TEM image of Fig. 2(A). It is interesting to note that a high dispersion of cluster-like NiS was found in Fig. S4, and the average size of the cluster was estimated to be ~ 2.3 nm. Figure 2(B) shows the HR-TEM image of the hollow sphere NiS nanomaterials. The value of lattice fringes was estimated to be 0.27 nm, correspond to the ascription of the crystalline plane of (101) NiS. The SAED pattern was recorded for the obtained hollow sphere NiS nanomaterials and is shown in Fig. 2(C). The resulting SAED pattern of the hollow sphere NiS nanomaterials had not shown any clear lattice fringes to investigate further the crystalline facets and *d* values, suggesting that the developed NiS in this study was amorphous crystalline structures. Figure S5 shows the EDX spectrum of the hollow sphere NiS nanomaterials, illustrated the existence of Ni and S in the region. The atomic ratio was further estimated based on the EDX spectrum of the NiS nanomaterials to be 64.5:35.5 which is well agreed with Fig. S2.

The chemical compositions and the valence states of the as-prepared hollow sphere NiS nanomaterials were further analyzed with XPS technique. Figure 3 presents the high-resolution XPS spectra for Ni 2P and S2P for the hollow sphere NiS nanomaterials. The core-level XPS Ni spectrum (Fig. 3(A)) exhibited a couple of major peaks at 855.9 and 861.7 eV, originally generating from $Ni2_{P1/2}$ and $Ni2_{P3/2}$for Ni^{2+} in the NiS nanomaterials [33, 35, 36]. The other two peaks at 861.3 and 879.7 eV were ascribed to satellite peaks for NiS nanomaterials. Figure 3(B) presents the S 2P spectrum of the NiS nanomaterials. The major XPS peaks were observed at

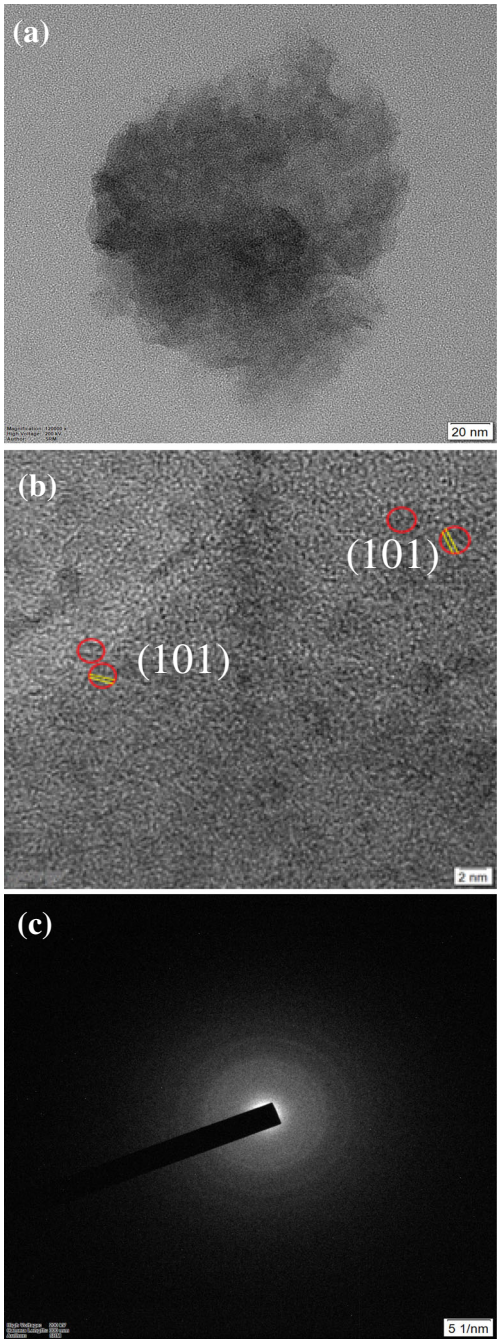

Fig. 2 TEM (**a**) and HR-TEM (**b**) images of the HS-NiS nanomaterials; (**c**) SAED pattern of the HS-NiS nanomaterials

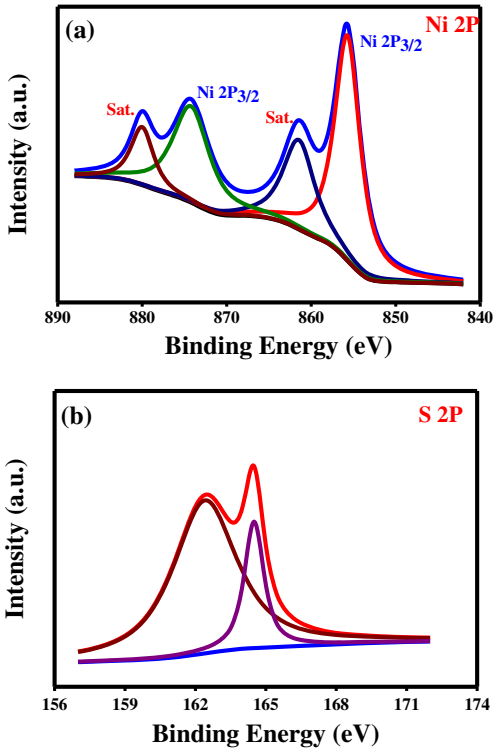

Fig. 3 XPS spectra of the Ni 2p (**a**), and S 2p (**b**) regions for the HS-NiS nanomaterials

163.6 and 168.3 eV, corresponding to the binding energies of S^{2-} [37]. The atomic composition ratio of Ni and S was measured to be 6.5: 3.5 for NiS nanomaterials. The XPS results of Fig. 3 further confirmed the existence of NiS. The crystalline nature of the developed hollow sphere NiS nanomaterials was further studied with XRD analysis. Figure S6 presents the XRD pattern of the developed hollow sphere NiS nanomaterials modified NiF (red curve) and bare NiF (black curve) electrodes. The small peaks observed at 2 values of ~ 18.3° and ~ 27.2°were ascribed to (110) and (220) hexagonal crystalline plane of NiS [33, 38]. The other major peaks marked with star (*) were derived from the NiF substrate.

Electrochemical characterization of hollow sphere NiS nanostructures

The electrochemical characteristics of the hollow sphere NiS nanomaterials were further studied with a cyclic voltammetric technique under alkaline medium. Figure S7 presents the CV curves of the NiF (a) and NiF modified with HS-NiS (NiF/HS-NiS) (c) electrodes recorded at different scan rates, starting from 10 to 125 mV s^{-1} under 1.0 M KOH in the electrochemical potential window of − 0.2 to 0.65 V (vs Ag/AgCl). As expected, a pair of electrochemical oxidation and reduction peaks were observed in the potential range of 0.1–0.5 V for the NiF and NiF/HS-NiS electrodes, ascribed to the Ni^{2+}/Ni^{3+} redox couple [33]. It is noted that the CV curves area of the NiF/HS-NiS electrode is much higher by ~ 4 times in comparison to bare NiF, suggesting that NiF/HS-NiS electrode possessed a larger double-layer capacitance. As shown in Fig. S7, the anodic and cathodic currents were increased as the square root of scan rates increases, showing that both bare NiF and NiF/HS-NiS electrodes exhibited the diffusion-controlled process under alkaline electrolyte. It is further exposed that there is no substantial change in the amount of the electrochemically active species involved in the electrochemical redox reactions. The electrochemical active surface area (ECASA) of the NiF/HS-

NiS electrode (Fig. S8) was estimated to be ~ 1.43 cm^2 based on the equation of R_fS [39], where R_f is the roughness factor, and S stands for the geometric surface area of the electrode.

Electrocatalytic oxidation of lactic acid at the hollow sphere NiS nanostructures

The electrocatalytic activity of the developed NiF/HS-NiS electrode was tested towards the oxidation of lactic acid. Figure 4(a) displays the CV curves of the bare NiF and NiF/HS-NiS electrodes recorded in the presence (solid curve) and absence (dotted curve) of 10.0 mM lactic acid at a scan rate of 20 mV s^{-1} in the potential window of − 0.2 to 0.6 V (vs Ag/AgCl). As shown in Fig. 4(a), the anodic peak current (i_a) was increased about ~ 1.34 mA at the potential of ~ 0.52 V after the addition of 10.0 mM lactic acid due to the ascription of the electrochemical oxidation of lactic acid. However, there was no significant enhancement of the anodic current observed at the bare NiF electrode as presented in Fig. 4(a). Figure 4(b) shows the CV curves of the NiF/HS-NiS electrode recorded with various scan rates in the presence of 10.0 mM lactic acid. As can be seen in Fig. 4(c), a linear plot was observed on the plotting of anodic currents against the square root of the scan rates, suggesting that the electrochemical oxidation of lactic acid was mediated by the diffusion of electroactive species at the NiF/HS-NiS electrode. As expected, the electrochemical oxidation of lactic acid at the NiF/HS-NiS electrode is an irreversible process. The electrochemical rate of the reaction towards the lactic acid oxidation at the NiF/HS-NiS, and bare NiF electrodes was estimated to be ~ 1.63×10^{-3}, and ~ 0.36×10^{-3} mol s^{-1} cm^2, respectively. During the electrochemical oxidation of lactic acid, lactate is formed electrochemically, followed by the chemical reaction of lactate to pyruvic acid (Eqs. 3 and 4). The active Ni^{2+}species is initially converted to Ni^{3+} species during the anodic scan through the electrochemical oxidation reaction. The as-formed Ni^{3+} species rapidly oxidizes the lactic acid molecules to lactate via two-electron transfer process [40].

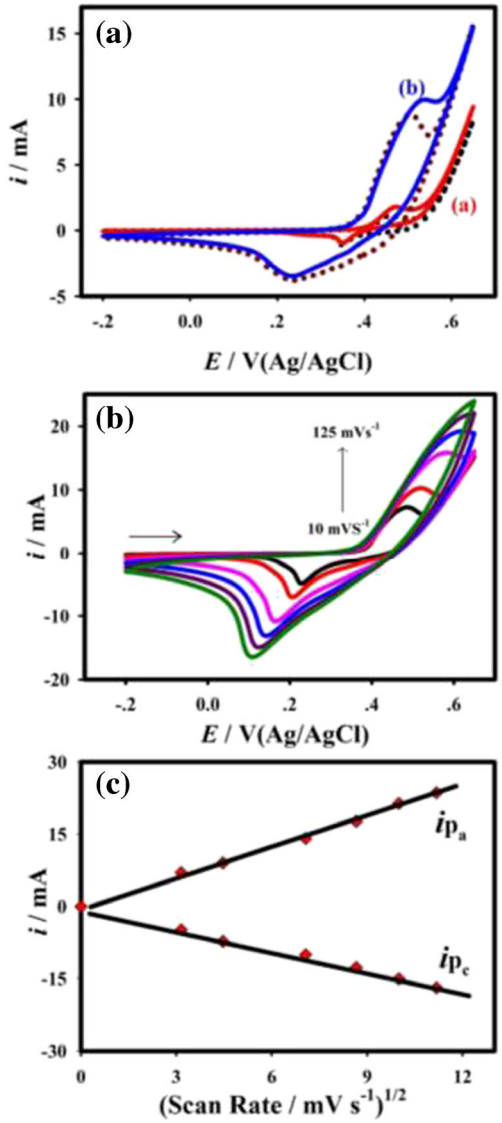

Fig. 4 CV curves of the bare NiF (curve a, red color) and NiF/HS-NiS (curve b, blue curve) electrodes recorded in the absence (dotted lines) and presence of 10.0 mM lactic acid in 1.0 M KOH at a scan rate of 20 mV s^{-1}

$$Ni^{2+} \rightarrow Ni^{3+} + e^- \quad (3)$$

$$Ni^{3+} + LA \rightarrow Ni^{2+} + \text{Pyruvic Acid} \quad (4)$$

Electroanalytical performance of the hollow sphere NiS nanostructures

The electrochemical detection of lactic acid was performed with an amperometric *i-t* technique based on the electrocatalytic activity of the NiF/HS-NiS electrode. Figure 5(a) depicts the current–time curves of the NiF/HS-NiS electrode recorded under 1.0 M KOH during the consecutive adding of lactic acid at regular intervals of 60 s at an applied electrode potential (E_{app}) of 0.50 V (vs Ag/AgCl). The applied potential (E_{app}) was chosen based on the electrocatalytic lactic acid oxidation potential (Fig. 4(a)). The anodic current was steadily increased after the addition of various concentrations of lactic acid, starting from 0.5 to 88.5 μM due to the association of lactic acid oxidation at the NiF/HS-NiS electrode. The limit of detection (LOD) was estimated as 0.023 μM based on the equation of $3\sigma/b$ where σ means the standard deviation of the blank and b represents the slope of the calibration curve. The steady-state current response was obtained within 3 s following each addition of lactic acid. Figure 5(b) displays the corresponding calibration plot of Fig. 5(a). The linear relationship was attained for the anodic currents against the lactic acid concentration, which was observed in the concentration range from 0.5 to 88.5 μM with a correlation coefficient of $R^2 = 0.98$ and a sensitivity of

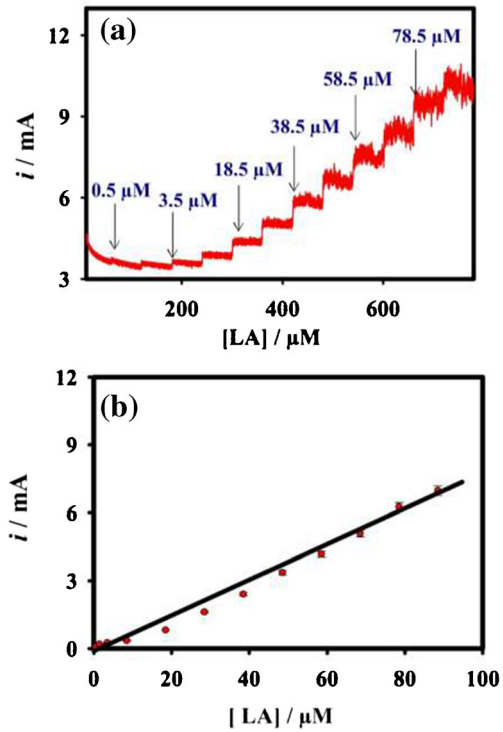

Fig. 5 (**a**) Amperometric *i-t* response of the NiF/HS-NiS electrode recorded in 1.0 M KOH under various lactic acid concentrations, starting from 0.5 to 88.5 μM, E_{app}: 0.50 V. (**b**) Corresponding calibration plot of measured anodic current against lactic acid concentrations

0.655 μA μM^{-1} cm^{-2}. The obtained low calibration regression was due to the high double-layer capacitance of the developed NiF/HS-NiS electrode. To our knowledge, the present sensor based on hollow sphere NiS nanomaterials exhibited such a lowest detection limit and high sensitivity against the detection of lactic acid. To show the merit of this non-enzymatic amperometric sensor, a list of recent electrochemical lactic sensor was summarized in Table 1. It is highly evident that the hollow sphere NiS nanomaterials demonstrated the lowest detection limit and the highest sensitivity in comparison with reported sensors [41–50]. The attained high performance of the electrochemical sensing attribution was due to the association of the good electrocatalytic aptitude of hollow sphere NiS nanomaterials.

The selectivity of the developed sensor was tested with various interferences such as uric acid (UA), ascorbic acid (AA), paracetamol (PA), Mg^{2+}, Na^{+}, and Ca^{2+} with 100-fold higher concentration when compared to lactic acid concentration. The potential interferences were chosen because of their excessive presence in real human urine samples. Figure 6 displays the amperometric *i-t* response of the NiF/HS-NiS electrode towards the 10.0 μM lactic acid in the presence of 1.0 mM uric acid (UA), ascorbic acid (AA), paracetamol (PA), Mg^{2+}, Na^{+}, and Ca^{2+}. The relative amperometric response to lactic acid at the NiF/HS-NiS electrode in the absence and in the presence of potential interferences are shown in Fig. 6(b). It is suggested that the developed NiF/HS-NiS electrode in the present study exhibited good selectivity to lactic acid without using any enzymes on the electrode surface, mimicking the enzymatic activity. The stability of the lactic acid sensor based on NiF/HS-NiS electrode was performed by conducting the amperometric technique in the presence of 10.0 mM LA at the constant applied potential of 0.50 V over 5000 s under alkaline electrolyte. As presented in Fig. S9, a plot of the measured catalytic current versus time showed that the anodic current was slightly decreased by less than ~ 7%, which was due to the ascription of adsorption of oxidized products of lactic acid. The developed electrochemical lactic acid sensor based on NiF/HS-NiS electrode possessed good durability.

The precision of the lactic acid sensor was performed by repeating the electrocatalytic oxidation of 10.0 mM lactic acid

Table 1 Comparison of the performance of various non-enzymatic lactic acid sensors with the sensor fabricated in the present work sensing electrode

Materials	Technique	Sensitivity	Linear range	LOD	Ref.
AuR-DTSP-LO_x	Amperometry	1.49 μA mM^{-1}	0.1 mM - 1.3 mM	3.93 μM	[44]
MWCNT/MB	Amperometry	3.46 μA cm^{-2} mM^{-1}	0.10–10.0 mM	7.5 μM	[49]
Fe_3O_4/MWCNT	Amperometry	7.67 μA mM^{-1}	50.0–500.0 μM	5.0 μM	[50]
LDH/CeO_2/GCE	Amperometry	571.19 μA mM^{-1}	0.2–2.0 mM	50.0 μM	[48]
LO_x/SWCNT	Amperometry	9.4 μA mM^{-1} cm^{-2}	0.01–0.9 mM	3.0 μM	[51]
CoPC-SPCE	Amperometry	–	74.0 μM −1.5 mM	18.3 μM	[52]
NiO NPS	Amperometry	–	0.01–5.0 mM	5.7 μM	[53]
GCE/MIP	Amperometry	1.9×10^5 μA M^{-1}	0.1–15.0 nM	0.0089 nM	[23]
GCE/Co_3O_4	Amperometry	–	0.05–3.0 mM	6.0 μM	[11]
HS-NiS	Amperometry	0.65 μA μM^{-1} cm^{-2}	0.5–88.5 μM	0.023 μM	This Work

Au NPS, gold nanoparticles; *GCE*, glassy carbon electrode; *LDH*, lactate dehydrogenase; *LOx*, lactate oxidase; *MWCNT*, multi-walled carbon nanotubes; *PPY*, polypyrrole; *Pt*, platinum; *Pttca*, poly-5,2′−5′−2″-terthiophene-3′-carboxylic acid; *LDA*, lactate dehydrogenase

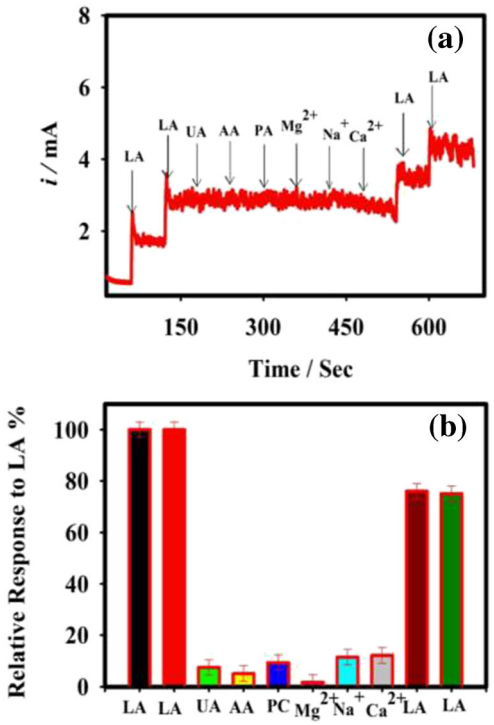

Fig. 6 Amperometric *i-t* responses of the NiF/HS-NiS electrode recorded in 1.0 M KOH with the addition of 10.0 μM lactic acid, 1.0 mM uric acid, 1.0 mM ascorbic acid, 1.0 mM paracetamol, 1.0 mM Mg^{2+}, 1.0 mM Na^{+}, 1.0 mM Ca^{2+}, and 10.0 μM lactic acid at E_{app}: 0.50 V. (**b**) Measured relative response of the NiF/HS-NiS electrode in the presence of various interferences

under alkaline electrolyte at the NiF/HS-NiS electrode. The resulting relative standard deviation (RSD) was estimated to be 2.3% for three individual measurements. In addition, the present electrochemical sensor exhibited the repeatability of ~ 90% for three successive measurements. Thus, the developed NiF/HS-NiS-based lactic acid sensor exhibited good precision.

Application to human urinary samples

Furthermore, the developed NiF/HS-NiS based sensing electrode was successfully verified to validate its ability towards the detection and determination of lactic acid in real human urine samples by using the standard addition method (SAM). In this SAM, prior to the addition of lactic acid in urine samples was considered as the baseline or zero concentration of analyte for the recovery values of lactic acid concentrations ranged from 0.5 to 2.0 μM. The resulting recovery values of the lactic acid in a human urine sample at the NiF/HS-NiS electrodes are listed in Table 2. The recovery values of the lactic acid in human urinary were reached in the range of 97.3–99.2% with relative standard deviation (RSD %) values between 1.2 and 1.6, suggesting that the established sensing electrode based on hollow sphere NiS nanostructures possessed a strong prospective to empower applications in clinical and biomedical analyses.

Table 2 Recovery tests of lactic acid in actual human urine samples ($n = 3$) at the NiF/HS-NiS

Material	Added/ μM	Found[a]/ μM	Recovery/ %	RSD/ %
HS-NiS	0.50	0.49	99.2	1.49
	1.0	0.97	97.3	1.16
	2.0	1.96	98.2	1.59

[a] Average of three measurements

Conclusion

In the present study, we have reported a facile, one-step and green electrochemical approach to fabricate hollow sphere NiS nanostructures based sensing electrode towards the high-performance lactic acid detection for the first time. The developed hollow sphere NiS nanostructures exhibited an outstanding electrocatalytic activity towards the lactic acid oxidation through the unique hollow sphere surface morphology, highly exposed electrochemical active sites in the absence of any binder, enzyme mimic electrocatalytic activity and huge electrochemical active surface area. Thus, the hollow sphere NiS nanostructured sensing electrode delivered a low detection limit, fast response time, high sensitivity, and wide linear range. The present sensor exhibited selectivity without the utilization of any enzymes in the presence of a variety of potential interferences such as uric acid (UA), ascorbic acid (AA), paracetamol (PA), Mg^{2+}, Na^{+}, and Ca^{2+}. The sensor based on NiF/HS-NiS electrode was furthermore successfully performed in real human urine samples to distinguish selectively, revealing its potential practicability. The present study is not only present a novel approach for the electrochemical fabrication of the hollow sphere NiS nanostructured sensing electrode but also offers a promising enzyme-free electrochemical sensor towards the detection of lactic acid in human urine. Moreover, further sensing experiment tests using cell lines, organs, and other biological systems are requisite towards the development of a next-generation electrochemical lactic acid sensor device for various clinical and biomedical applications.

Acknowledgements Authors specially acknowledge to SRM Institute of Science and Technology (SRM IST) for providing all the research facilities, including SRM-SCIF for TEM measurements.

Funding information This work was supported by the Science and Engineering Research Board (SERB)-Start-up Research Grant (Ref. No.: SERB-SRG/2019/000123) and the Department of Science and Technology (DST)-Technology Mission Division (TMD) (Grant No.: DST/TMD/MES/2 K17/29), New Delhi.

Compliance with ethical standards

Conflict of interest The author(s) declare that they have no competing interests.

References

1. Bobade S, Kalorey DR, Warke S (2016) Biosensor devices: a review on their biological applications. Biosci Biotechnol Res Commun 9:132–137. https://doi.org/10.21786/bbrc/19.1/20
2. Govindhan M, Adhikari BR, Chen A (2014) Nanomaterials-based electrochemical detection of chemical contaminants. RSC Adv 4: 63741–63760. https://doi.org/10.1039/c4ra10399h
3. Krishnan SK, Singh E, Singh P, Meyyappan M, Nalwa HS (2019) A review on graphene-based nanocomposites for electrochemical and fluorescent biosensors. RSC Adv 9:8778–8781. https://doi.org/10.1039/c8ra09577a
4. Napi MLM, Sultan SM, Ismail R, How KW, Ahmad MK (2019) Electrochemical-based biosensors on different zinc oxide nanostructures: a review. Materials (Basel) 12:1–34. https://doi.org/10.3390/ma12182985
5. Shavanova K, Bakakina Y, Burkova I, Shtepliuk I, Viter R, Ubelis A, Beni V, Starodub N, Yakimova R, Khranovskyy V (2016) Application of 2D non-graphene materials and 2D oxide nanostructures for biosensing technology. Sensors (Switzerland) 16:1–23. https://doi.org/10.3390/s16020223
6. Khan I, Saeed K, Khan I (2019) Nanoparticles: properties, applications and toxicities. Arab J Chem 12:908–931. https://doi.org/10.1016/j.arabjc.2017.05.011
7. Ansari AA, Alhoshan M, Alsalhi MS, Aldwayyan AS (2010) Nanostructured metal oxides based enzymatic electrochemical biosensors. Biosensors. https://doi.org/10.5772/7201
8. Huang H, Su S, Wu N, Wan H, Wan S, Bi H, Sun L (2019) Graphene-based sensors for human health monitoring. Front Chem 7:1–26. https://doi.org/10.3389/fchem.2019.00399
9. Monosik R, Stredansky M, Tkac J, Sturdik E (2012) Application of enzyme biosensors in analysis of food and beverages. Food Anal Methods 5:40–53. https://doi.org/10.1007/s12161-011-9222-4
10. Dandan Z, Ke Z, Minghui Y (2019) Gold nanoparticle-loaded hollow Prussian blue nanoparticles with peroxidase-like activity for colorimetric determination of L-lactic acid. Microchim Acta 186(2):121
11. Abdul SC, Nusrat NM, Sidra A, Fouzia C, Umair A, Muhammad I et al (2019) Facile non-enzymatic lactic acid sensor based on cobalt oxide nanostructures. Electroanalysis 31(7):1296–1303
12. Yao Y, Li H, Wang D, Liu C, Zhang C (2017) An electrochemiluminescence cloth-based biosensor with smartphone-based imaging for detection of lactate in saliva. Analyst 142:3715–3724. https://doi.org/10.1039/c7an01008g
13. Prakash S, Chakrabarty T, Singh AK, Shahi VK (2013) Polymer thin films embedded with metal nanoparticles for electrochemical biosensors applications. Biosens Bioelectron 41:43–53. https://doi.org/10.1016/j.bios.2012.09.031
14. Seenivasan R, Chang W, Gunasekaran S (2015) Highly sensitive detection and removal of lead ions in water using cysteine-functionalized graphene oxide/polypyrrole nanocomposite film electrode. https://doi.org/10.1021/acsami.5b03904
15. Lawal AT (2018) Author' s accepted manuscript. Biosens Bioelectron 106:149–178. https://doi.org/10.1016/j.bios.2018.01.030
16. Zhao F, Zeng J, Shih WC (2017) Nanoporous gold nanocomposites as a versatile platform for plasmonic engineering and sensing. Sensors (Switzerland) 17:1–11. https://doi.org/10.3390/s17071519
17. Betancourt T, Brannon-Peppas L (2006) Micro-and nanofabrication methods in nanotechnological medical and pharmaceutical devices. Int J Nanomedicine 1:483–495. https://doi.org/10.2147/nano.2006.1.4.483
18. Malekian B, Xiong K, Emilsson G, Andersson J, Fager C, Olsson E, Larsson-Langhammer E, Dahlin A (2017) Fabrication and characterization of plasmonic nanopores with cavities in the solid support. Sensors (Switzerland) 17:1–11. https://doi.org/10.3390/s17061444
19. Ahmad R, Wolfbeis OS, Hahn YB, et al (2018) Deposition of nanomaterials: a crucial step in biosensor fabrication
20. Othman A, Karimi A, Andreescu S (2016) Functional nanostructures for enzyme based biosensors: properties, fabrication and applications. J Mater Chem B 4:7178–7203. https://doi.org/10.1039/C6TB02009G
21. Govindhan M, Chen A (2016) Enhanced electrochemical sensing of nitric oxide using a nanocomposite consisting of platinum-tungsten nanoparticles, reduced graphene oxide and an ionic liquid. Microchim Acta 183:2879–2887. https://doi.org/10.1007/s00604-016-1936-y
22. Govindhan M, Amiri M, Chen A (2015) Au nanoparticle/graphene nanocomposite as a platform for the sensitive detection of NADH in human urine. Biosens Bioelectron 66:474–480. https://doi.org/10.1016/j.bios.2014.12.012
23. Pereira TC, Stradiotto NR (2019) Electrochemical sensing of lactate by using an electrode modified with molecularly imprinted polymers, reduced graphene oxide and gold nanoparticles. Microchim Acta 186(12):764
24. Dandan Z, Congsen W, Junjun L, Minghui YD (2019) C_3N_4 nanosheet-supported Prussian blue nanoparticles as a peroxidase mimic: colorimetric enzymatic determination of lactate. Microchim Acta 186(11):735
25. Tonelli D, Scavetta E, Gualandi I (2019) Electrochemical deposition of nanomaterials for electrochemical sensing. Sensors (Switzerland) 19. https://doi.org/10.3390/s19051186
26. Wang J (2012) Electrochemical biosensing based on noble metal nanoparticles. Microchim Acta 177:245–270. https://doi.org/10.1007/s00604-011-0758-1
27. Xia X, Zhang Y, Chao D, Guan C, Zhang Y, Li L, Ge X, Bacho IM, Tu J, Fan HJ (2014) Solution synthesis of metal oxides for electrochemical energy storage applications. Nanoscale 6:5008–5048. https://doi.org/10.1039/c4nr00024b
28. Li H, Huang M, Cao G (2017) Magnetic properties of atomic 3d transition-metal chains on S-vacancy-line templates of monolayer MoS2: effects of substrate and strain. J Mater Chem C 5:4557–4564. https://doi.org/10.1039/c6tc04672j
29. Wang Y, Guo J, Wang T, Shao J, Wang D, Yang YW (2015) Mesoporous transition metal oxides for supercapacitors. Nanomaterials 5:1667–1689. https://doi.org/10.3390/nano5041667
30. Chen H, Jiang J, Zhang L, Wan H, Qi T, Xia D (2013) Highly conductive NiCo2S4 urchin-like nanostructures for high-rate pseudocapacitors. Nanoscale 5:8879–8883. https://doi.org/10.1039/c3nr02958a
31. Verma M, Yadav R, Sinha L, Mali SS, Hong CK, Shirage PM (2018) Pseudocapacitive-battery-like behavior of cobalt manganese nickel sulfide (CoMnNiS) nanosheets grown on Ni-foam by electrodeposition for realizing high capacity. RSC Adv 8:40198–40209. https://doi.org/10.1039/C8RA07471B
32. Feng LL, Yu G, Wu Y, Li GD, Li H, Sun Y, Asefa T, Chen W, Zou X (2015) High-index faceted Ni3S2 nanosheet arrays as highly active and ultrastable electrocatalysts for water splitting. J Am Chem Soc 137:14023–14026. https://doi.org/10.1021/jacs.5b08186
33. Li X, Shang X, Rao Y, Dong B, Han GQ, Hu WH, Liu YR, Yan KL, Chi JQ, Chai YM, Liu CG (2017) Tuning crystal phase of NiS x through electro-oxidized nickel foam: a novel route for preparing

efficient electrocatalysts for oxygen evolution reaction. Appl Surf Sci 396:1034–1043. https://doi.org/10.1016/j.apsusc.2016.11.084
34. Pang H, Wei C, Li X, Li G, Ma Y, Li S, Chen J, Zhang J (2014) Microwave-assisted synthesis of NiS2 nanostructures for supercapacitors and cocatalytic enhancing photocatalytic H2 production. Sci Rep 4:1–8. https://doi.org/10.1038/srep03577
35. Jana S, Samai S, Mitra BC, Bera P, Mondal A (2014) Nickel oxide thin film from electrodeposited nickel sulfide thin film: peroxide sensing and photo-decomposition of phenol. Dalton Trans 43: 13096–13104. https://doi.org/10.1039/c4dt01658k
36. Chhetri M, Sultan S, Rao CNR (2017) Electrocatalytic hydrogen evolution reaction activity comparable to platinum exhibited by the Ni/Ni(OH) 2 /graphite electrode. Proc Natl Acad Sci U S A 114: 8986–8990. https://doi.org/10.1073/pnas.1710443114
37. Bhosale R, Kelkar S, Parte G, Fernandes R, Kothari D, Ogale S (2015) NiS1.97: a new efficient water oxidation catalyst for photoelectrochemical hydrogen generation. ACS Appl Mater Interfaces 7:20053–20060. https://doi.org/10.1021/acsami.5b05077
38. Tong F, Wu X, Jia W, Guo J, Pan Y, Lv Y, Jia D, Zhao X (2020) NiS nanosheets with novel structure anchored on coal-based carbon fibers prepared by electrospinning for flexible supercapacitors. CrystEngComm. 22:1625–1632. https://doi.org/10.1039/c9ce01560d
39. Wang XD, Xu YF, Rao HS, Xu WJ, Chen HY, Zhang WX, Kuang DB, Su CY (2016) Novel porous molybdenum tungsten phosphide hybrid nanosheets on carbon cloth for efficient hydrogen evolution. Energy Environ Sci 9:1468–1475
40. Elakkiya R, Maduraiveeran G (2019) A three-dimensional nickel-cobalt oxide nanomaterial as an enzyme-mimetic electrocatalyst for the glucose and lactic acid oxidation reaction. New J Chem 43: 14756–14762
41. Gao W, Yin H, Nyein Y et al (2016) Heavy metal monitoring of body fluids a wearable microsensor array for multiplexed heavy metal monitoring of body fluids. https://doi.org/10.1021/acssensors.6b00287
42. Bravo I, Revenga-Parra M, Pariente F, Lorenzo E (2017) Reagentless and robust biosensor for direct determination of lactate in food samples. Sensors (Switzerland) 17:1–11. https://doi.org/10.3390/s17010144
43. Shankar SS, Shereema RM, Rakhi RB (2018) Electrochemical determination of adrenaline using MXene/graphite composite paste electrodes. ACS Appl Mater Interfaces 10:43343–43351. https://doi.org/10.1021/acsami.8b11741
44. Gamero M, Sosna M, Pariente F, Lorenzo E, Bartlett PN, Alonso C (2012) Influence of macroporous gold support and its functionalization on lactate oxidase-based biosensors response. Talanta 94:328–334. https://doi.org/10.1016/j.talanta.2012.03.051
45. Giménez-Gómez P, Gutiérrez-Capitán M, Capdevila F, Puig-Pujol A, Fernández-Sánchez C, Jimenez-Jorquera C (2017) Miniaturized flow-system integrating enzymatic electrochemical biosensors for monitoring the malolactic fermentation of red wines. Proceedings 1: 787. https://doi.org/10.3390/proceedings1080787
46. Jiang D, Chu Z, Peng J, Jin W (2016) Screen-printed biosensor chips with Prussian blue nanocubes for the detection of physiological analytes. Sensors Actuators B Chem 228:679–687. https://doi.org/10.1016/j.snb.2016.01.076
47. Mohiuddin M, Arbain D, Islam AKMS, Ahmad MS, Ahmad MN (2016) Alpha-glucosidase enzyme biosensor for the electrochemical measurement of antidiabetic potential of medicinal plants. Nanoscale Res Lett 11:1–12. https://doi.org/10.1186/s11671-016-1292-1
48. Nesakumar N, Sethuraman S, Krishnan UM, Rayappan JBB (2013) Fabrication of lactate biosensor based on lactate dehydrogenase immobilized on cerium oxide nanoparticles. J Colloid Interface Sci 410:158–164. https://doi.org/10.1016/j.jcis.2013.08.009
49. Pereira AC, Aguiar MR, Kisner A, Macedo DV, Kubota LT (2007) Amperometric biosensor for lactate based on lactate dehydrogenase and Meldola blue coimmobilized on multi-wall carbon-nanotube. Sensors Actuators B Chem 124:269–276. https://doi.org/10.1016/j.snb.2006.12.042
50. Teymourian H, Salimi A, Hallaj R (2012) Low potential detection of NADH based on Fe 3O 4 nanoparticles/multiwalled carbon nanotubes composite: fabrication of integrated dehydrogenase-based lactate biosensor. Biosens Bioelectron 33:60–68. https://doi.org/10.1016/j.bios.2011.12.031
51. Miraida P, Dámaris S, Nicole del T, Kai G (2015) A comparative study of different protein immobilization methods for the construction of an efficient nano-structured lactate oxidase-SWCNT-biosensor, Biosens Bioelectron 64:138–146
52. Takeshi S, Touru S, Masatoshi O, Tetsuji I, Taka-aki H (2012) Amperometric l-lactate biosensor based on screen-printed carbon electrode containing cobalt phthalocyanine, coated with lactate oxidase-mesoporous silica conjugate layer. Anal Chim Acta 714: 114–120
53. Sidra A, Aneela T, Amber S, Raffaello M, Zafar Hussain I, Alberto V (2019) A sensitive enzyme-free lactic acid sensor based on NiO nanoparticles for practical applications, anal. Methods 11:3578

Publisher's note Springer Nature remains neutral with regard to jurisdictional claims in published maps and institutional affiliations.